J Mater Sci: Mater Med (2008) 19:143–151
DOI 10.1007/s10856-007-3110-x

# Protein adsorption on materials for recording sites on implantable microelectrodes

**Jamunanithy Selvakumaran · Joseph L. Keddie · David J. Ewins · Michael Pycraft Hughes**

Received: 23 August 2005 / Accepted: 13 July 2006 / Published online: 21 June 2007


**Abstract** Implantable microelectrodes have the potential to become part of neural prostheses to restore lost nerve function after nerve damage. The initial adsorption of proteins to materials for implantable microelectrodes is an important factor in determining the longevity and stability of the implant. Once an implant is in the body, protein adsorption takes place almost instantly before the cells reach the surface of an implant. The aim of this study was to identify an optimum material for electrode recording sites on implantable microelectrodes. Common materials for electrode sites are gold, platinum, iridium, and indium tin oxide. These, along with a reference material (titanium), were investigated. The thickness and the structure of adsorbed proteins on these materials were measured using a combination of atomic force microscopy and ellipsometry. The adsorbed protein layers on gold (after 7 and 28 days of exposure to serum) were the smoothest and the thinnest compared to all the other substrate materials, indicating that gold is the material of choice for electrode recording sites on implantable microelectrodes. However, the results also show that indium tin oxide might also be a good choice for these applications.

J. Selvakumaran · D. J. Ewins · M. P. Hughes (✉)
Centre for Biomedical Engineering, School of Engineering, University of Surrey, Guildford, Surrey GU2 7XH, UK
e-mail: m.hughes@surrey.ac.uk

J. L. Keddie
Department of Physics, School of Electronics and Physical Science, University of Surrey, Guildford, Surrey GU2 7XH, UK

*Present Address:*
J. Selvakumaran
Department of Materials, Imperial College London, Exhibition Road, London SW7 2AZ, UK

**Keywords** Microelectrodes · Implantable · Metals · Protein adsorption · Recording sites · Ellipsometry

## Introduction

When permanent nerve damage occurs, the nerves proximal and distal to the point of damage often remain intact and active. In order to exploit this for the restoration of function, scientists have developed chronically implantable microelectrodes to record from and/or stimulate cells of the remaining nervous system [1]. Partial restoration of lost function has been achieved by advances in functional electrical stimulation [2]; however, restoration of complex functions such as standing and walking require a feedback loop to regulate the output of the stimulator. To this end, a number of groups have developed chronically implantable microelectrodes [3, 4] to record signals from the human peripheral nervous system. Similar microelectrodes structures have also been implanted in the central nervous system as part of neural prostheses; for example, a multielectrode array implanted in the motor cortex and surrounding areas has been developed to extract motor signals from the brain capable of controlling an artificial limb [5]. Figure 1 shows an electron micrograph of a typical implantable microelectrode probe, consisting of a number of electrode sites located on a penetrating shank that is inserted into a nerve. Typically, the electrode sites are made of a conducting metal deposited on a silicon-based substrate. The whole microelectrode is usually insulated by a passivation layer, leaving the electrode sites and bonding pads exposed.

Protein adsorption is believed to be the initial event that takes place when a material is inserted into the body [6, 7]. Since these initially adsorbed proteins play a significant

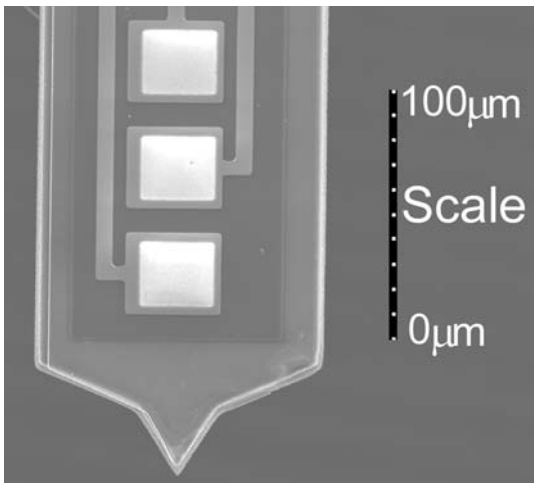


**Fig. 1** Scanning electron micrograph of a typical neuroprobe. Recording sites (pale squares) are exposed through a passivation layer following deposition onto a needle-shaped silicon substrate. The scale bar shows 100 μm; the probe is approximately 8 μm deep

influence on the subsequent adsorption of further proteins, cells, and microorganisms, they play a large role in dictating subsequent interfacial reactions and ultimately the biocompatibility of the material [8]. Protein adsorption is therefore of key significance in determining the in vivo performance of implants. In the case of electrode recording sites, there must be an intimate, physical contact between the nerve cells and electrodes in order to maximise the signal-to-noise ratio. To achieve this, the surface should be covered with the thinnest layer of protein possible. Furthermore, smoother surfaces are preferred to rougher surfaces, because rougher surfaces give rise to higher surface area, thus increasing the opportunity for microbes to adhere and cause infection.

Adsorption rates vary between different materials, and it is therefore necessary to assess the rate at which proteins adsorb to various candidate materials for recording sites in order to optimise the performance of a probe. Once in the body, an implant will be exposed to proteins and ions in the blood and extracellular fluid. Proteins and ions from the extracellular fluid are the first to be adsorbed to the implant, which then attract cells of the immune system and other cells to the implant surface. The constituents of diluted blood plasma closely resemble the constituents of extracellular fluid, and protein adsorption studies using diluted blood plasma therefore provide the closest match to the in vivo situation.

In this paper, we describe an assessment of protein adsorption from plasma onto typical materials used for implantable electrodes, through the combined use of atomic force microscopy (AFM) and spectroscopic ellipsometry. A number of materials in common use for chronically implantable microelectrodes were chosen for study: gold (Au), platinum (Pt), iridium (Ir), indium tin oxide (ITO) and titanium (Ti). Au, Pt, and Ir were selected because they are the most common materials used for in vivo electrode sites [4, 9–21]. ITO was chosen because of its wide use as in vitro planar electrodes for recording electrical signals from neurons [22–26]. Although Ti is not a very good electronic conductor, it was chosen as a reference material because it is a long established implant material [27] for which protein adsorption has already been well-characterised [28–30]. The materials were deposited as thin films (100 nm in thickness in most cases) to replicate the thin films used in implantable microelectrodes.

## Materials and methods

### Materials

All the materials except ITO were deposited as thin films (100 nm) on glass microscope slides (75 mm × 25 mm × 1 mm). The thickness of the ITO layer was 200 nm, prepared by a ''float'' process in which molten glass was floated on a pool of liquid tin under a nitrogen/hydrogen atmosphere (Delta Technologies, MN, USA). Au, Pt and Ti thin films were obtained from the University of Sheffield's (UK) EPSRC Central Facility for III–V Semiconductors. The Ir slides were obtained from Goodfellow (UK). The Au, Pt and Ir films were deposited over a 10 nm Ti interlayer to act as an adhesion layer to the glass substrate. Materials were cut to size (10 mm × 12 mm), cleaned with 70% ethanol and then washed three times with distilled water before all the experiments. The reverse side of the ITO slide used for ellipsometry was roughened using a fine sandpaper to prevent reflection from this interface.

### Methods

Rabbit plasma (Charles River, UK) was diluted in a 1:10 ratio with distilled water to give a final total protein concentration of 5 mg/mL. The total protein concentration of rabbit plasma was determined by using a Pierce BCA protein assay kit (cat # 23225) and Unicam SP 600 series-2 spectrophotometer. A standard curve was constructed using bovine serum albumin (BSA) standards measured against a measured optical density at 562 nm. The diluted plasma was preheated to 37 °C and centrifuged at 160 g for 5 min to remove any clumps of protein. The electrode materials were incubated in 8 mL of diluted plasma at 37 °C for either 1 day, 7 days or 28 days. At the end of the incubation period, samples were rinsed with 5 mL of distilled water and dried overnight in a desiccator.

*Ellipsometry*

Spectroscopic ellipsometry was used to measure the thickness of the protein film on materials exposed to plasma for 1 day. After 7 or 28 days of plasma exposure, the films were too thick to measure satisfactorily using ellipsometry. Ellipsometry relies on the measurement of the change in the polarisation state of light caused by reflection from an interface [31]. It is a highly sensitive means of determining the structure of organic interfacial layers [32]. Two parameters describe the change in the state of polarisation: $\Psi$ (which refers to the change in the relative amplitude of the light after reflections) and $\Delta$ (which refers to the change in the relative phase).

A variable angle-of-incidence spectroscopic ellipsometer with rotating analyser (J. A. Woollam Co., Inc., Lincoln, NE, USA) was used. Spectroscopic scans were performed on the material surfaces at wavelengths between 400 nm and 800 nm in steps of 10 nm, and at angles of incidence of 65°, 70° and 75°, before and after exposure to plasma. Measurements were taken five times for each material. The scans of the materials prior to plasma exposure were used to obtain their complex refractive index (both real (n) and imaginary (k) components) through inversion of the data.

Values of the thickness and roughness of the adsorbed protein layers were obtained by modelling the spectra using commercial software (WVASE32, J.A. Woollam Co. Inc.) that determined the minimum of the mean-squared error (MSE) of an optical model in describing the $\psi$ and $\Delta$ spectra. The dispersion of the real part of the refractive index, $n$, of the protein layer was described in the model by a Cauchy equation:

$$n(\lambda) = A + \frac{B}{\lambda^2},$$

in which $\lambda$ is the wavelength of light in μm, and $A$ and $B$ are both constants [33]. Through the preliminary analysis of several adsorbed films, standard values of $A = 1.55$ and $B = 0.01$ μm$^2$ were obtained for the protein. Over the range of wavelengths that were used, the protein was adequately described as transparent with $k = 0$. In the iterative fitting procedure to obtain the minimum MSE, the thickness and the roughness of the protein layer were varied. All of the metal films were sufficiently absorbing so that the optical constants of the glass substrate did not need to be considered in modelling the data. Because the ITO is transparent, however, its thickness and optical constants, as well as the optical constants of the glass substrates were determined independently and considered in the subsequent modelling.

*Atomic Force Microscopy (AFM)*

AFM was performed on all the materials to obtain topographic images of the surfaces prior to and after 1 day, 7 days and 28 days of exposure to plasma using a NanoScope IIIa (Digital Instruments, California) with silicon tips. A roughness analysis was performed on all the surfaces before and after exposure to plasma for 7 days. Tapping mode AFM was performed to scan across the surface, allowing both inspection and the determination of the mean and RMS roughness parameters ($R_a$ and $R_{rms}$ respectively). In order to assess the thickness of protein film adsorbed to materials after 7 days and 28 days, part of the protein film was carefully removed using cotton buds soaked in trypsin (0.25%) to create a step between the film and the substrate. The debris after trypsin treatment was removed using cotton buds soaked in 70% ethanol and the samples were allowed to air dry for 2 h. The scans were performed across the step using tapping mode AFM, and roughness and section analysis were performed across the created step.

## Results

### Analysis of bare surfaces

The surface energy and roughness are the two most important properties of a material in determining the adsorption of proteins [34]. In turn, the fabrication process plays a minor role in influencing the surface roughness of a thin film. The root-mean-square and average ($R_{rms}$ and $R_a$) of the materials are shown in Fig. 2. As the $R_{rms}$ is an indication of the deviation of height from the mean data plane, it gives a more useful description of the surface roughness compared to $R_a$. It can be seen that Ti had the

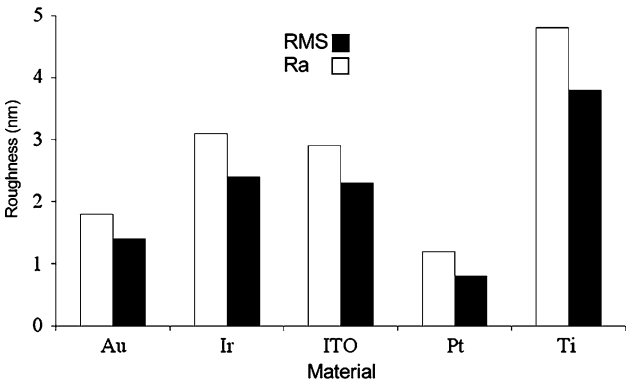


**Fig. 2** The surface roughness ($R_{rms}$ and $R_a$) of different materials, obtained from a 9 μm$^2$ area scan for each material by AFM

roughest surface and Pt had the smoothest surface. ITO and Ir had similar surface roughness values, which were in turn higher than Pt and Au. The surface roughness of Au was found to be approximately 60% lower than that of Ti, by both measures of surface roughness. The AFM images of all the bare surfaces are shown as image (a) in Figs. 3, 4, 5, 6, 7. Analysis indicated that Ti showed the highest amount of surface features (peaks and valleys), whilst Pt showed the lowest amount of surface features. ITO and Ir had similar surfaces. It can be seen that both Au and Pt had regular grain structures, but the grains were larger in the Au sample when compared to the Pt sample.

In addition to the above studies, a qualitative assessment of surface free energy was performed (data not shown) by depositing 1 μL distilled water onto the surface of the bare substrates and measuring the diameter of the droplet forming on the surface. The diameter of the water drop is related to the hydrophilicity of the substrate; as a general indicator, the larger the diameter of the droplet, the more hydrophilic the surface is and the greater the surface free energy. The tests indicated that the surface free energy of Ti and ITO were significantly greater than those of Au, Ir and Pt, which were similar to one another.

## Materials exposed to plasma for 1 day

Tapping mode AFM was performed on all the materials after 1-day incubation with plasma. Representative topography images are shown as image (b) in Fig. 3–7. Au and Pt were found to have more uniform surfaces than all the other materials, which correlates with the smooth and regular grain structures seen on the topography images of both bare surfaces. Ir had the highest amount of surface features with deep valleys and high peaks. Although ITO has a high amount of surface features, it can be seen from the contrast in the images that they are not as deep as the surface features seen on Ir or Ti. The thickness of protein films was obtained from ellipsometry data by measuring Ψ and Δ and building a model to fit these parameters. The ellipsometry results for the five materials are shown in Fig. 8 and 9. The thinnest layer of protein is initially adsorbed on ITO, whilst a layer that was approximately five times thicker adsorbed on Ti. Ti showed a high degree of variation in the thickness of the protein layer adsorbed to it, indicated by the high standard deviation (indicated in the figure by the vertical bar).

## Materials after 7 and 28 days exposure to plasma

At longer exposure times, ellipsometry was found to give unsatisfactory results due to the thickness of the film, and so tapping mode AFM was used to determine topography and protein thickness on all the materials after 7 and 28 days incubation with plasma. The topography images for 7-day exposure are shown in Figs. 3(c)–7 (c). As can be seen, Au and Pt had smoother surfaces than the other materials. Ir and Ti had significantly more pronounced surface features than the other materials. ITO in particular

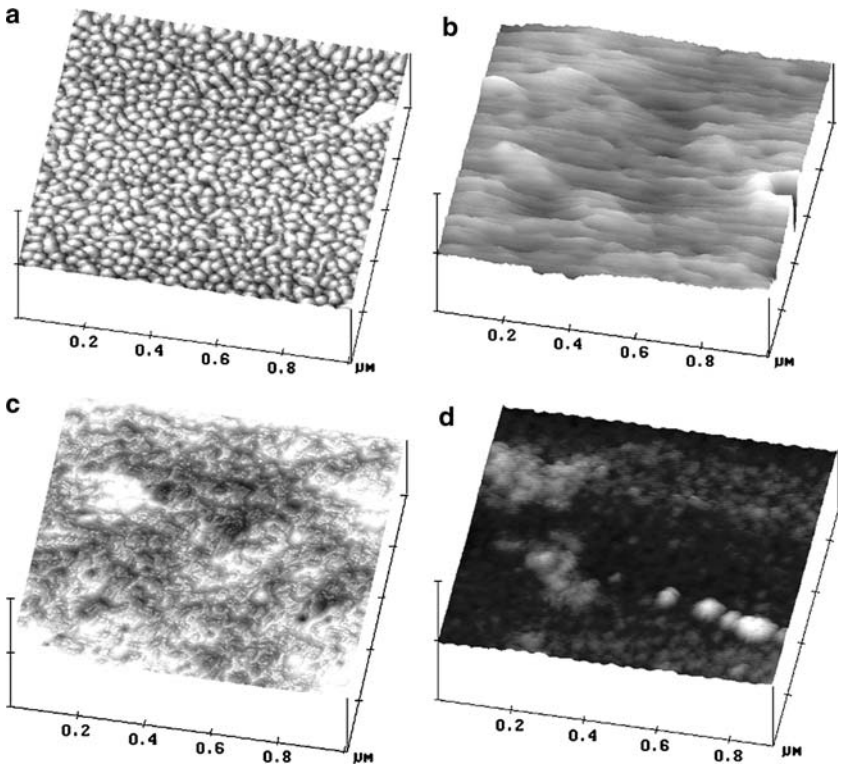


**Fig. 3** AFM topography images of Au. (**a**) bare substrate, and (**b**) 1 day, (**c**) 7 days, and (**d**) 28 days exposure to plasma. Scales shown on each figure apply to x- and y-directions (images are square); z-scale for all images is 200 nm

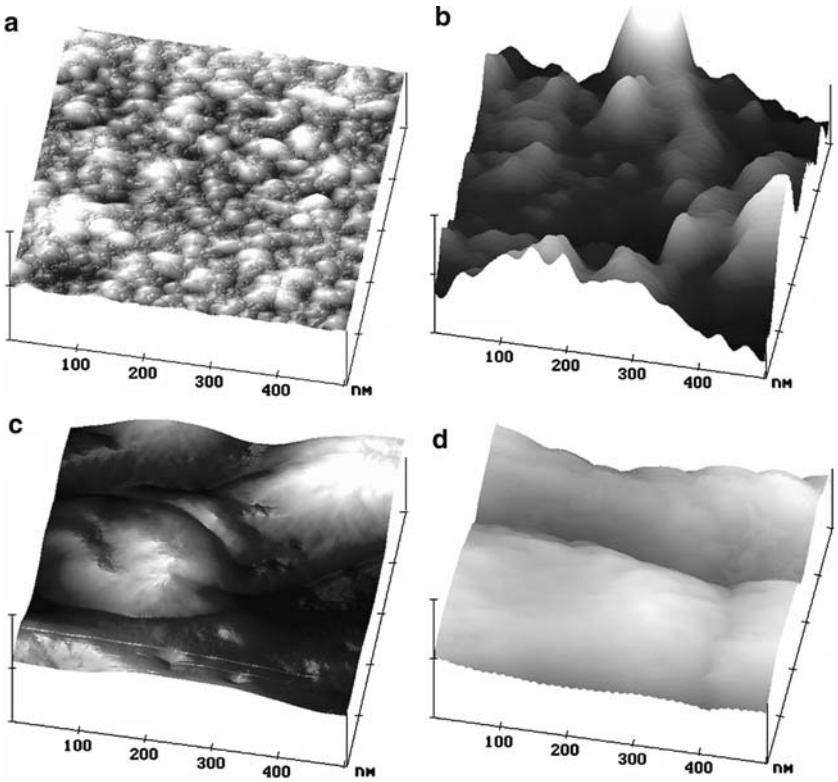


**Fig. 4** AFM topography images of Ir. (**a**) bare substrate, and (**b**) 1 day, (**c**) 7 days, and (**d**) 28 days exposure to plasma. Scales shown on each figure apply to x- and y-directions (images are square); z-scale for all images is 100 nm

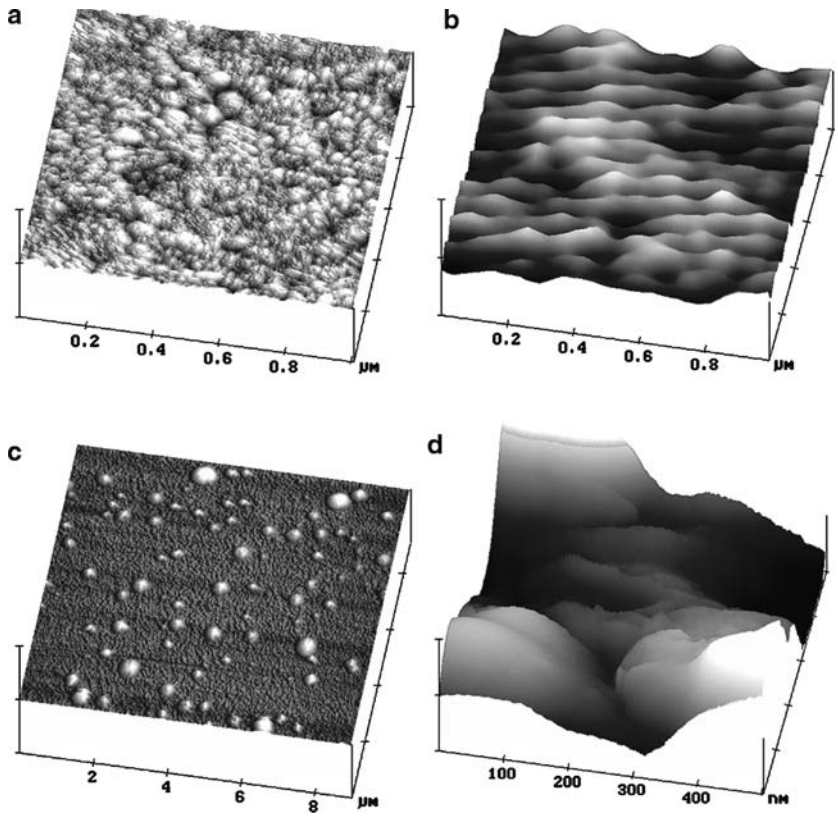


**Fig. 5** AFM topography images of ITO. (**a**) bare substrate, and (**b**) 1 day, (**c**) 7 days, and (**d**) 28 days exposure to plasma. Note that scales are different to show detail of island formation. Scales shown on each figure apply to x- and y-directions (images are square); (**a**) and (**b**) scan size 1 μm, z-scale 200 nm; (**c**) scan size 9 μm, z-scale 2 μm; (**d**) scan size 500 nm, z-scale 100 nm

showed hemispherical island structures scattered across the surface. The thickness of protein layer adsorbed to different materials after 7 days exposure to plasma is shown in Fig. 9, and the roughness of the protein layer adsorbed to different materials after 7 days exposure to plasma is shown in Fig. 10. Tapping mode AFM was also performed

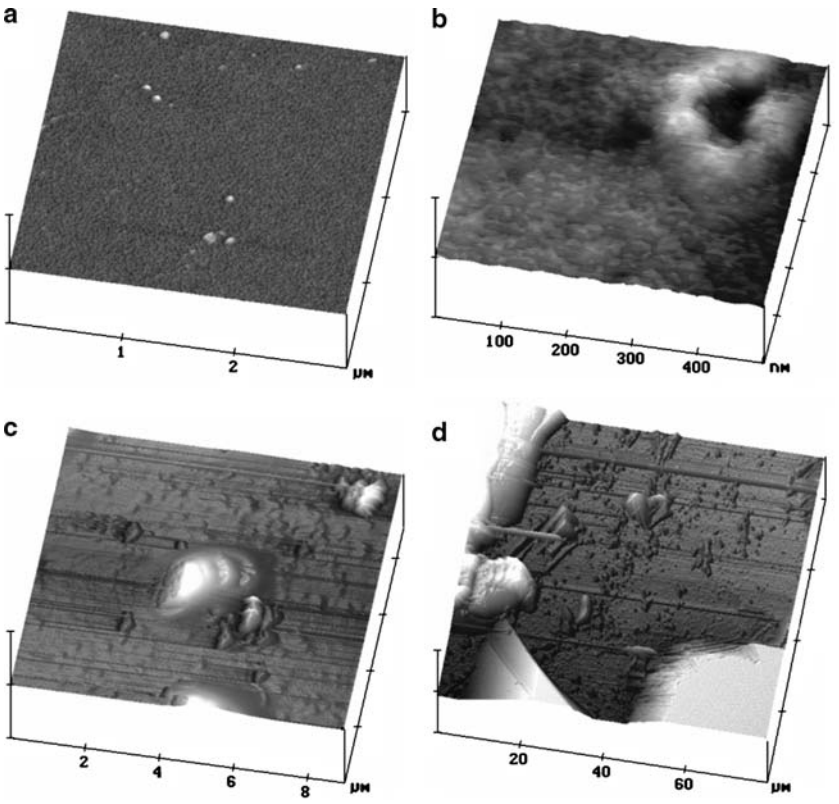


**Fig. 6** AFM topography images of Pt. (**a**) bare substrate, and (**b**) 1 day, (**c**) 7 days, and (**d**) 28 days exposure to plasma. Scales shown on each figure apply to x- and y-directions (images are square), and differ to show delamination detail at longer time intervals. z-scales are 500 nm, 100 nm, 2 μm, 10 μm respectively

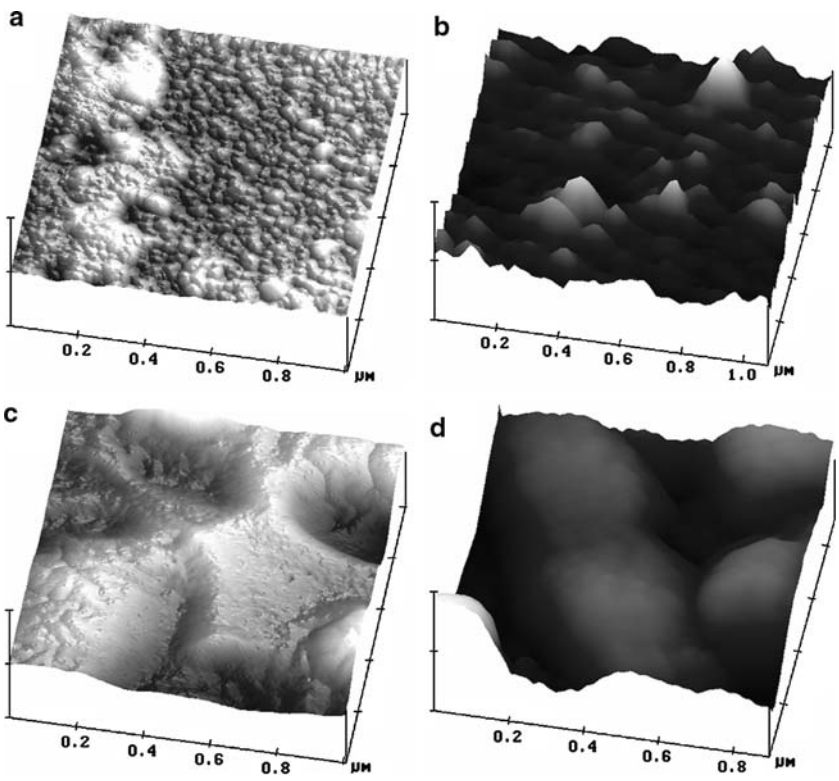


**Fig. 7** AFM topography images of Ti. (**a**) bare substrate, and (**b**) 1 day, (**c**) 7 days, and (**d**) 28 days exposure to plasma. Scales shown on each figure apply to x- and y-directions (images are square); scan size is 1 μm, z-scale 200 nm

on all the materials after 28 days exposure to plasma. The topography images are shown in Figs. 3(d)–7(d). As can be seen Ir, Ti and ITO all had significant surface features when compared to Au. Pt had the most significant surface features when compared to all the materials. The thickness of protein layer adsorbed to different materials after

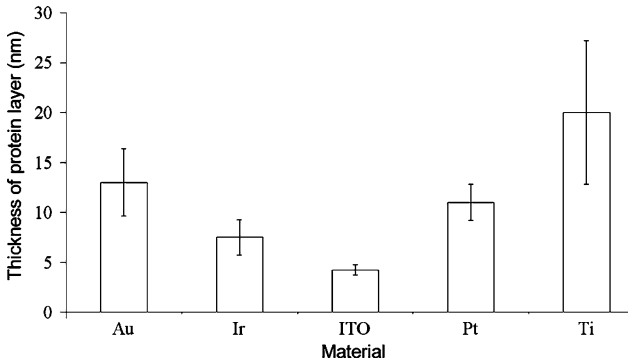


**Fig. 8** The mean thickness ($n = 3$) of the adsorbed protein layer adsorbed to the different materials after exposure to plasma for 1 day, as measured using ellipsometry. The vertical bars indicate one standard deviation from the mean

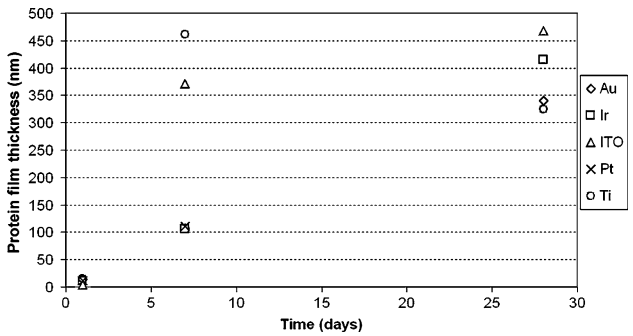


**Fig. 9** A plot showing the variation in the thickness of the protein layer adsorbed to different materials after 1, 7, and 28 days exposure to plasma, as measured using a combination of ellipsometry (for 1 day exposure) and step-technique AFM (for 7 and 28 day exposures)

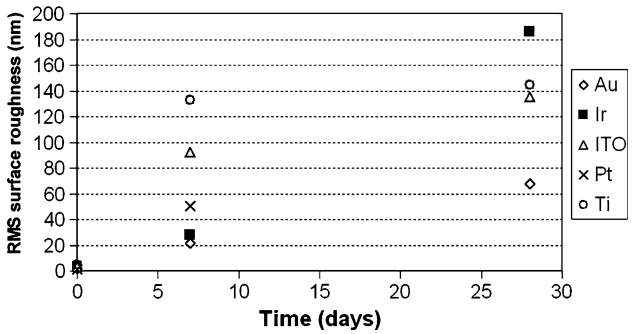


**Fig. 10** A plot of the variation in RMS surface roughness ($R_{rms}$) of the bare substrate prior to exposure, and following 7 and 28 days exposure to plasma, taken using AFM analysis for the range of different materials used in this study

28 days exposure to plasma is shown in Fig. 9, and the roughness of the protein layers adsorbed to different materials after 28 days exposure to plasma is shown in Fig. 10.

## Discussion

In all cases (and as shown in Fig. 9), the thickness of protein layer adsorbed after 7 days was higher than that after 1 day exposure to plasma, indicating a growth process. The thickness of protein layer adsorbed to Au, Ir, and Pt after 7 days was similar, indicating the rate of adsorption is similar on these three materials up to 7 days and which in turn correlates well with their similar values of surface energy. The rate of protein adsorption onto ITO and Ti was much faster over the first 7 days compared to other materials, again correlating well with the surface energy measurements. As can be seen from the topography images, the Au and Pt samples had an apparently continuous layer with uniform thickness after 7 days exposure to plasma, whereas Ti and Ir showed peak and valley structures, and ITO showed distinctive island-like structures scattered across the surface. The smoother protein layer seen deposited on Au could be explained by the lower surface roughness, and the coarser protein layer on Ti may be explained by the higher surface roughness of the bare substrates. This possibly indicates that both the topography and surface energy of the bare substrate have a role in dictating the manner in which protein is adsorbed, but have distinct roles in dictating the protein film thickness and topography respectively.

After 28 days of exposure, protein adsorption became more variable between materials. Pt has the highest rate of adsorption between 7 and 28 days, though this could be partly attributed to delamination seen on parts of this sample, some of which is visible in the AFM image (Fig. 6). The results have been removed from Figs. 9 and 10 as it is quite likely that they are not representative of the protein layer. After 28 days exposure to plasma, Au has the smoothest and most continuous layer, ITO has non-uniform features, whereas all the other materials have high peaks and deep valley structures; in the case of Ti this was significant enough to produce a roughness value similar to ITO.

Although the mechanisms of the protein adsorption process have been studied and reviewed extensively, many aspects of the mechanisms of the adsorption process remain speculative due to the technical difficulties of observing the process [35, 36]. It is known that fibrous capsules ultimately reach a stable thickness when the body has encapsulated a foreign object to isolate it from the rest of the body, but a number of mechanisms have been suggested for how this might occur. For example, some reports in the literature describe protein adsorption as the irreversible adsorption of protein, whereas other researchers have stated that desorption can also occur [37, 38]. The extent of reversibility of protein adsorption depends on the surface energy, surface coverage, and extent of

denaturation; protein adsorption to hydrophilic substrates is generally reversible [34]. An alternative explanation could be that there is no desorption, but instead there is a re-arrangement of the protein molecules to create a denser packing.

If we consider the stabilisation process as being based on protein adsorption and desorption, Ti was found to have the thickest layer of protein after 7 days and thinnest layer of protein after 28 days, possibly indicating that after an initial adsorption process, the rate of desorption exceeded rate of adsorption between 7 days and 28 days, resulting in a thinner film after the longer time period. The rate of protein adsorption onto Au and Ir slowed considerably during the 7–28 day period, indicating that if both adsorption and desorption are taking place, the rate of adsorption was slightly higher than the rate of desorption. Similarly, the rate of protein adsorption onto ITO after 7 days was significantly lower than the rate of adsorption before 7 days, indicating both adsorption and desorption processes with rate of adsorption dominating over the rate of desorption, though the unusual method of island formation may also play a role in this.

From the surface energy experiments Ti is the most hydrophilic surface compared to other surfaces and the pattern of protein adsorption on Ti correlates with this. All the other materials are more hydrophobic than Ti and hence show more permanent protein adsorption. The exception to this is the case of ITO, but the deposition pattern—consisting of large island structures with little protein deposited between—indicates that the deposition mechanism onto this semiconducting material is quite dissimilar to those of the other materials, and is worthy of further study. In our results, the material with the roughest and most hydrophilic surface (Ti) adsorbed the thickest layer of protein after 1 day and the thinnest layer of protein after 28 days. The material with the lowest surface energy (Au) adsorbed the thinnest and smoothest layer of protein, and the material with the highest surface energy (Ti) adsorbs the thickest and roughest layer of protein after 7 days exposure to plasma. This indicates that the use of Au, being among the more common electrode material, is an excellent choice but also indicates that ITO, largely used for in vitro experimentation on account of its transparency, may also be a good choice for acute in vivo applications.

## Conclusions

This work is the first to compare the protein adsorption on different materials specifically for microelectrode sites on implantable microelectrodes. We conclude that Au is the material of choice for electrode recording sites on implantable microelectrodes due to its minimal protein encapsulation of all those analysed. However, this work has also demonstrated the suitability of other materials, and particularly ITO, for applications in electrode sites on implantable microelectrodes.

**Acknowledgements** The authors wish to thank the EPSRC for a scholarship for JS. The authors also wish to thank Dr Geoff Hill at the University of Sheffield, EPSRC central facility for III–V semiconductors for thin film preparation, and Dr Peter Zhdan for assistance with the AFM, and Prof John Watts for valuable discussions.

## References

1. P. HEIDUSCHKA and S. THANOS, *Prog. Neurobio.* **55** (1998) 433–461
2. P. H. PECHHAM, J. T. MORTIMER and E. B. MARSOLAIS, *Ann. Biomed. Eng.* **8** (1980) 369–388
3. G. ENSELL, D. J. BANKS, D. J. EWINS, W. BALACHANDRAN and P. R. RICHARDS, *J. Microelectromech. Sys.* **5** (1996) 117–121
4. G. ENSELL, D. J. BANKS, P. R. RICHARDS, W. BALACHANDRAN and D. J. EWINS, *Med. Biol. Eng. Comp.* **38** (2000) 175–179
5. P. J. ROUSCHE and R. A. NORMAN, *J. Neurosci. Meth.* **82** (1998) 1–15
6. J. D. ANDRADE and V. HLADY, *Ann. N. Y. Acad. Sci.* **516** (1987) 158–172
7. M. WAHLGREN and T. ARNEBRANT, *Tibtech* **9** (1991) 201–208
8. D. F. WILLIAMS, I. N. ASKILL and R. J. SMITH, *Biomed. Mater. Res.* **19** (1985) 313–320
9. S. L. BEMENT, K. D. WISE, D. J. ANDERSON, K. NAJAFI and K. L. DRAKE, *IEEE Trans. Biomed. Eng.* **33**(1986) 230–241
10. D. J. EDELL, *IEEE Trans. Biomed. Eng.* **33** (1986) 203–214
11. K. L. DRAKE, K. D. WISE, J. FARRAYE, D. J. ANDERSON and S. L. BEMENT, *IEEE Trans. Biomed. Eng.* **35** (1988) 719–732
12. A. JONZON, E. N. LARSSON, P. A. OBERG and G. SEDIN, *Med. Biol. Eng. Comp.* **26** (1988) 624–627
13. J. ROZMAN, B. PIHLAR, P. STROJNIK and J. SCAND, *Rehab. Med. Suppl.* **17** (1988) 99–103
14. D. J. ANDERSON, K. NAJAFI, S. J. TANGHE, D. A. EVANS, K. L. LEVY, J. F. HETKE, X. XUE, J. J. JAPPIA and K. D. WISE, *IEEE Trans. Biomed. Eng.* **36** (1989) 693–704
15. K. NAJAFI, J. JI and K. D. WISE, *IEEE Trans. Biomed. Eng.* **37** (1990) 1–10
16. N. A. BLUM, G. CARKHUFF, H. K. CHARLES, R. L. EDWARDS and R. MEYER *IEEE Trans. Biomed. Eng.* **38** (1991) 68–74
17. R. M. BRADLEY, R. H. SMOKE, T. AKIN and K. NAJAFI, *Brain Res.* **594** (1992) 84–90
18. D. J. EDELL, V. V. TOI, V. M. MCNEIL and L. D. CLARK *IEEE Trans. Biomed. Eng.* **39** (1992) 635–643
19. A. C. HOOGERWERF and K. D. WISE, *IEEE Trans. Biomed. Eng.* **41** (1994) 1136–1146
20. C. KIM and K. D. WISE, *IEEE J. Slid-State Circuits* **31** (1996) 1230–1238
21. D. T. KEWLEY, M. D. HILLS, D. A. BORKHOLDER, I. E. OPRIS, N. I. MALUF, C. W. STORMENT, J. M. BOWER and G. T. A. KOVACS, *Sens. Actuat. A.* **58** (1997) 27–35
22. A. LITKE and M. MEISTER, *Nucl. Instrum. Meth. Phys. Res. A-Acc. Spectrom. Detect. Assoc. Equip.* **310** (1991) 389–394

23. Y. JIMBO and A. KAWANA, *Bioelectroch. Bioener.* **29** (1992) 193–204
24. G. W. GROSS, B. K. RHOADES, D. L. REUST and F. U. J. SCHWALM, *Neurosci. Meth.* **50** (1993) 131–143
25. M. GRATTAROLA, M. BOVE, G. VERRESCHI, S. MARTINOLA, M. TEDESCO and S. CHIARUGI, *Minerva Biotecnol.* **7** (1995) 228–233
26. K. V. GOPAL and G. W. GROSS, *Acta Oto-Laryngologica* **116** (1996) 690–696
27. M. M. KLINGER, F. RAHEMTULLA, C. W. PRINCE, L. C. LUCAS and J. E. LEMONS, *Crit. Rev. Oral Biol. Med.* **9** (1998) 449–463
28. E. BESS, R. CAVIN, K. MA and J. L. ONG, *Implant Dent.* **8** (1999) 126–32
29. F. HÖÖK, J. VÖRÖS, M. RODAHL, R. KURRAT, P. BÖNI, J. J. RAMSDEN, M. TEXTOR, N. D. SPENCER, P. TENGVALL, J. GOLD and B. KASEMO, *Colloid. Surfaces B.* **24** (2002) 155–170
30. Y. YANG, R. CAVIN and J. L. ONG, *J Biomed. Mater. Res.* **67A** (2003) 344–349
31. R. M. A. AZZAM and N. M. BASHARA, ''Ellipsometry and polarised light'' (North-Holland, Amsterdam, 1977)
32. J. L. KEDDIE, *Curr. Opin. Coll. Interf. Sci.* **6** (2001) 102–110
33. B. PARBHOO, S. IZRAEL, J. M. SALAMANCA and J. L. KEDDIE, *Surf. Interf. Anal.* **29** (2000) 341–345
34. T. A. HORBETT and J. L. BRASH in ''Proteins at interfaces: physicochemical and biochemical studies''. J. L. BRASH, T. A. HORBETT Eds. (ACS, Washington, DC, 1987) pp 1–36
35. J. D. ANDRADE and V. HLADY, *Adv. Polym. Sci.* **79** (1986) 1–63
36. T. A. HORBETT and J. L. BRASH, (1995) ACS symposium series 602, Washington, DC
37. T. P. BURGHARDT and D. AXELROD, *Biophys. J.* **33** (1981) 455–467
38. R. D. TILTON, C. R. ROBERTSON and A. P. J. GAST, *J. Colloid Interf. Sci.* **137** (1990) 192–203